ACS Pharmacology & Translational Science

pubs.acs.org/ptsci

Article

Inhibition of Severe Acute Respiratory Syndrome Coronavirus 2 Replication by Hypertonic Saline Solution in Lung and Kidney Epithelial Cells

Rafael R. G. Machado,[¶] Talita Glaser,[¶] Danielle B. Araujo, Lyvia Lintzmaier Petiz, Danielle B. L. Oliveira, Giuliana S. Durigon, Alessandra L. Leal, João Renato R. Pinho, Luis C. S. Ferreira, Henning Ulrich,* Edison L. Durigon,* and Cristiane Rodrigues Guzzo*

Cite This: https://doi.org/10.1021/acsptsci.1c00080

Read Online

ACCESS | Metrics & More | Article Recommendations

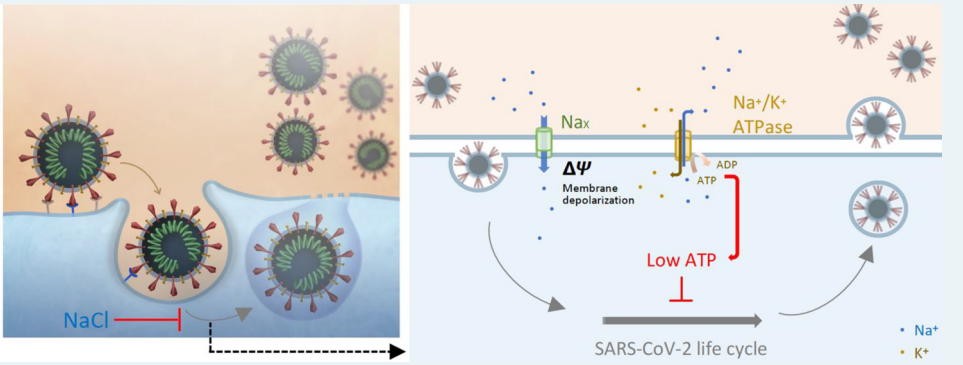

ABSTRACT: An unprecedented global health crisis has been caused by a new virus called severe acute respiratory syndrome coronavirus 2 (SARS-CoV-2). We performed experiments to test if a hypertonic saline solution was capable of inhibiting virus replication. Our data show that 1.2% NaCl inhibited virus replication by 90%, achieving 100% of inhibition at 1.5% in the nonhuman primate kidney cell line Vero, and 1.1% of NaCl was sufficient to inhibit the virus replication by 88% in human epithelial lung cell line Calu-3. Furthermore, our results indicate that the inhibition is due to an intracellular mechanism and not to the dissociation of the spike SARS-CoV-2 protein and its human receptor. NaCl depolarizes the plasma membrane causing a low energy state (high ADP/ATP concentration ratio) without impairing mitochondrial function, supposedly associated with the inhibition of the SARS-CoV-2 life cycle. Membrane depolarization and intracellular energy deprivation are possible mechanisms by which the hypertonic saline solution efficiently prevents virus replication *in vitro* assays.

KEYWORDS: *SARS-CoV-2, NaCl, virus inhibition, cell depolarization, ATP*

The world is facing a pandemic situation due to the pathogenic SARS-CoV-2 (Severe Acute Respiratory Syndrome CoronaVirus 2).[1] So far there have been more than 116 million confirmed patients around the world, and more than 2.6 million deaths due to COVID-19 disease, according to WHO data as of March 2021 (https://covid19.who.int). This new virus is an unprecedented serious global health threat, and few medical procedures are available which could reduce viral load, decreasing patient hospitalization time, virus dissemination, and the number of patients with severe symptoms. Different vaccines are available, but the new variants of SARS-CoV-2 may decrease their effectiveness.[2,3]

SARS-CoV-2 uses a surface glycosylated spike (S) protein to bind human angiotensin-converting enzyme 2 (hACE-2)[4] and may also with other host receptors such as CD147[5] and sialic acid receptors[6,7] to develop coronavirus disease (COVID-19). In the case of SARS-CoV, which shares 76% identity with the SARS-CoV-2 S protein, it has been suggested that the virus may also bind to host cells through DC-SIGN or L-SIGN receptors.[8,9] SARS-CoV-2 and ACE-2 interaction is essential to mediating virus infection.[10] The S protein has two main subunits, the S1 subunit involved in binding to the host cell receptor and the S2 subunit that mediates fusion of the viral and cellular membranes. Initially, the homotrimeric S protein

Received: March 15, 2021

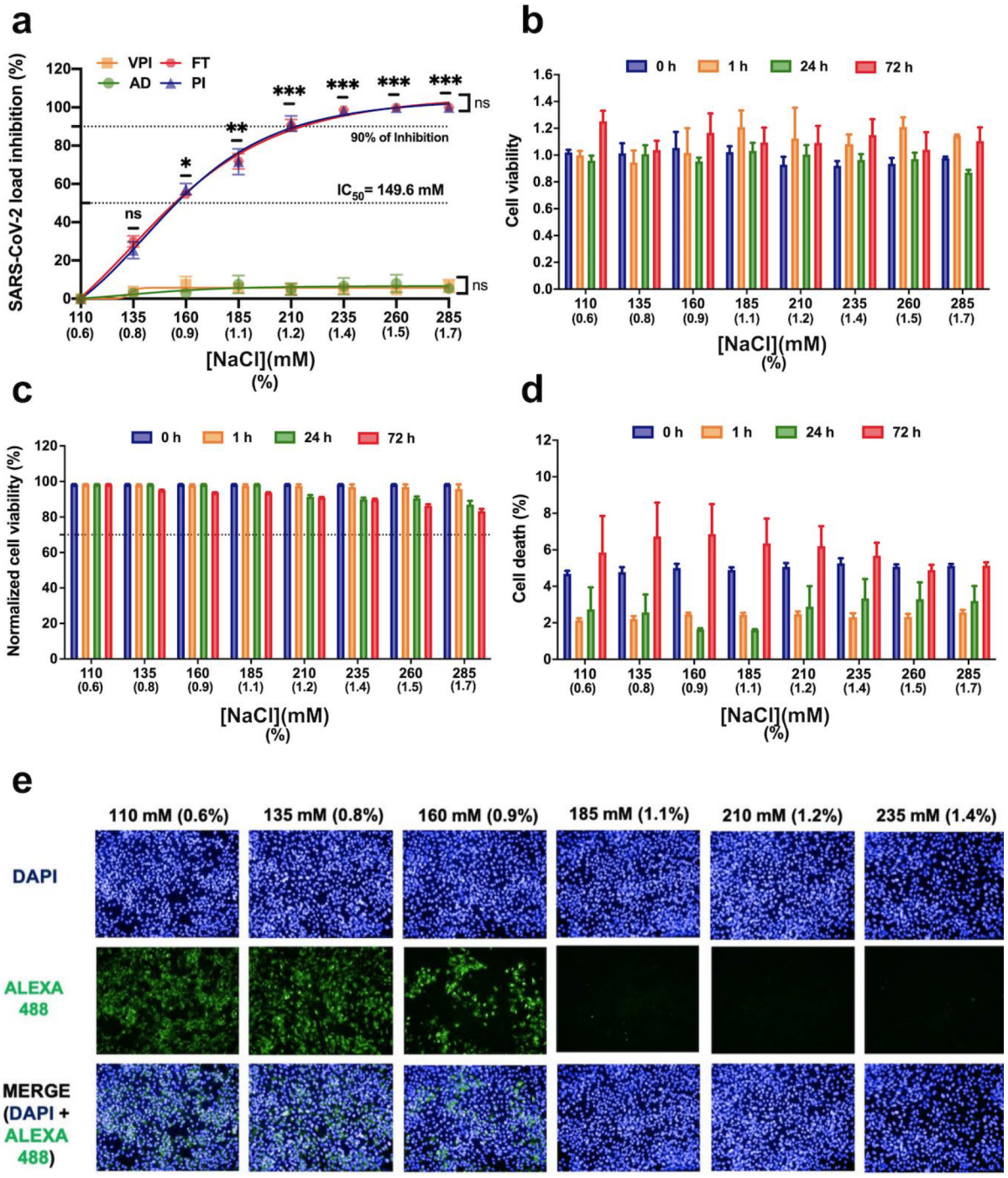

Figure 1. Antiviral activity of NaCl against SARS-CoV-2 in vitro assay. (a) *Y* axis labeling of the graph represents percentage inhibition of virus load in cellular supernatant by increasing NaCl concentration. Four different times of NaCl addition were evaluated, comprising the virus preincubation (VPI, orange line), absorption (AD, green line), postinfection (PI, blue line), and adsorption plus postinfection (FT, red line). Error bars indicate the standard error of the mean of three independent experiments with each one carried out in triplicate. *$p < 0.05$, **$p < 0.005$, and ***$p < 0.0005$ when compared to 110 mM NaCl. Vero CCL-81 cell viability was not significantly impaired in the presence of increasing concentrations of NaCl (110 mM up to 285 mM). (b) Cell viability was determined following 0, 1, 24, and 72 h post-treatment with different concentrations of NaCl using AlamarBlue Cell Viability Reagent (Thermo Fisher Scientific). (c) Cell viability was also determined by quantification of LDH released into the culture supernatant from cells with damaged membranes, using the CytoTox 96 Non-Radioactive Cytotoxicity Assay (Promega Corp., Madison, WI). Cell viability was normalized to that determined with cells kept at a physiological NaCl concentration (110 mM NaCl). (d) Percentage of dead cells determined by propidium iodide/Hoechst 33342 staining. Viability below 70% (cell death rates of more than 30%) was considered as evidence of cytotoxicity. Error bars represent the mean ± SEM of three independent experiments carried out in triplicate. (e) Infected cells by SARS-CoV-2 were observed by indirect immunofluorescence (IIF) assay. SARS-CoV-infected and noninfected Vero cells were stained with a convalescent serum, followed by incubation with the Alexa488-conjugated goat antihuman IgG antibody (green). Cells were counterstained with DAPI for nuclear staining (blue). Positive (infected nontreated cells) and negative (noninfected cells) controls are represented in the bottom of the image. Representative images were captured with a 20× objective using the Operetta High Content Imaging System (PerkinElmer).

https://doi.org/10.1021/acsptsci.1c00080
ACS Pharmacol. Transl. Sci. XXXX, XXX, XXX−XXX

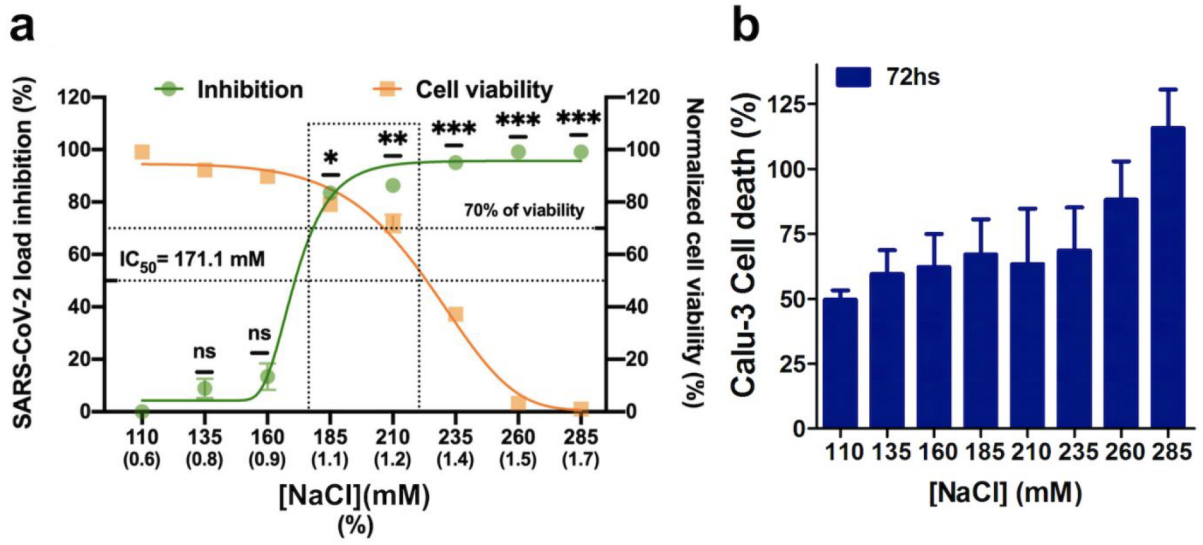

Figure 2. Effects of increasing NaCl concentrations on Calu-3 cells (lung epithelial cells). (a) The left *Y*-axis of the graph represents percentage inhibition of virus load in postinfection cellular supernatant. Error bars indicate the standard error of the mean of three independent experiments, each of them carried out in triplicate. *p < 0.05, **p < 0.005, and ***p < 0.0005 when compared to 110 mM NaCl. Cells were treated with increasing concentrations of NaCl (110 mM up to 285 mM). Then, 72 h post-treatment cellular viability was determined. The dotted rectangular area (185 to 210 mM NaCl) shows the concentrations of NaCl that significantly inhibit SARS-CoV-2 replication, and more than 70% of the cells are viable. (b) Percentage of dead cells determined via propidium iodide/Hoechst 33342 staining. Viability below 70% (cell death more than 30%) was considered as evidence of cytotoxicity. Error bars represent the mean ± SEM of three independent experiments carried out in triplicate.

via its receptor binding domain (RBD) located at the S1 subunit binds to hACE-2, causing a conformational change in the S1 and S2 subunits leading to the fusion of the virus membrane with the host cell membrane.[11,12] The SARS-CoV-2 S protein structure has been recently solved in the apo form[13] and in complex with ACE-2 protein.[14] Interestingly, the interface between the RBD of S protein with hACE-2 is highly polar, involving charged residues mainly located at the hACE-2 interface and polar residues at the RBD interface.[14] These ionic interactions might in principle be weakened by increasing the ionic strength of the environment and might be used to break down the interaction of the virus with the host cell. However, increasing NaCl concentration did not significantly affect RBD−hACE-2 binding affinity.[15] This may be explained by the way that RBD binds hACE-2. The RBD has two regions, E1 and E2, which bind to hACE-2 differently. At high ionic strengths, the hydrophilic contacts mediated by E2 become progressively weaker, while the hydrophobic contacts mediated by E1 increase to favor the maintenance of the Spike/hACE-2 complex. This may reflect the necessity of complex stability during the process of S1 subunit release followed by the virus−cell membrane fusion process.[15]

Nevertheless, the potential antiviral activity, *in vitro*, of sodium chloride (NaCl) has been already confirmed for RNA viruses, such as mengovirus,[14,16] respiratory syncytial virus, influenza A virus, human coronavirus 229E, and coxsackievirus B3, and also for DNA viruses, like herpes simplex virus-1 and murine gammaherpesvirus 68.[17] Furthermore, a randomized controlled clinical trial studying the effectiveness of the treatment for viral upper respiratory tract infection, using hypertonic saline nasal irrigation and gargle (HSNIG),[18] observed a decrease in the duration of illness, over-the-counter medications use, transmission within household contacts, and viral shedding.[18] However, the molecular details of the antiviral NaCl activity remain unresolved.

We performed different assays to determine if increasing NaCl concentrations would affect SARS-CoV-2 replication, an RNA enveloped virus, when cultured in monkey kidney epithelial cells (Vero CCL-81) as well as in a human lung cell line (Calu-3). We also performed assays to elucidate the mechanism involved in the action of NaCl in the inhibition of virus replication. In this study, we found that 1.5% NaCl inhibited virus replication by 100% in Vero cells, and 1.1% NaCl was sufficient to inhibit virus replication by 88% in Calu-3 cells. Our results indicate that the inhibition is due to an intracellular mechanism due to a low energy state, ATP deprivation, supposedly associated with inhibition of the SARS-CoV-2 life cycle. On the basis of our results, hypertonic saline solution efficiently prevents SARS-CoV-2 replication in *in vitro* assays and may be a promising therapeutic treatment for COVID-19 patients and an efficient way to prevent SARS-CoV-2 infection.

RESULTS

Antiviral Activity of Hypertonic Saline Solution against SARS-CoV-2 in Vero Cells. We determined effects of increasing concentrations of NaCl (135, 160, 185, 210, 235, 260, and 285 mM equivalent to 0.8, 0.9, 1.1, 1.2, 1.4, 1.5, 1.7%, respectively) on cell viability and their antiviral activity on SARS-CoV-2. Efficacies were evaluated by quantification of viral copy numbers in the cell supernatant using quantitative real-time RT-PCR (RT-qPCR) and confirmed by microscopic visualization of cytopathic effects following 72 h of infection (h.p.i.). Our data show that 210 mM NaCl (1.2%) was sufficient to inhibit virus replication by 90% (Figure 1a), achieving 100% of inhibition at 260 mM NaCl (1.5%). The inhibitory activity with a mean 50% inhibitory concentration (IC50) value was 149.6 mM. Next, to determine which stage of virus replication was affected by the NaCl, we evaluated if viral inhibition was a direct effect of NaCl on the virus particles. For that purpose, the viruses were preincubated with media

https://doi.org/10.1021/acsptsci.1c00080
ACS Pharmacol. Transl. Sci. XXXX, XXX, XXX−XXX

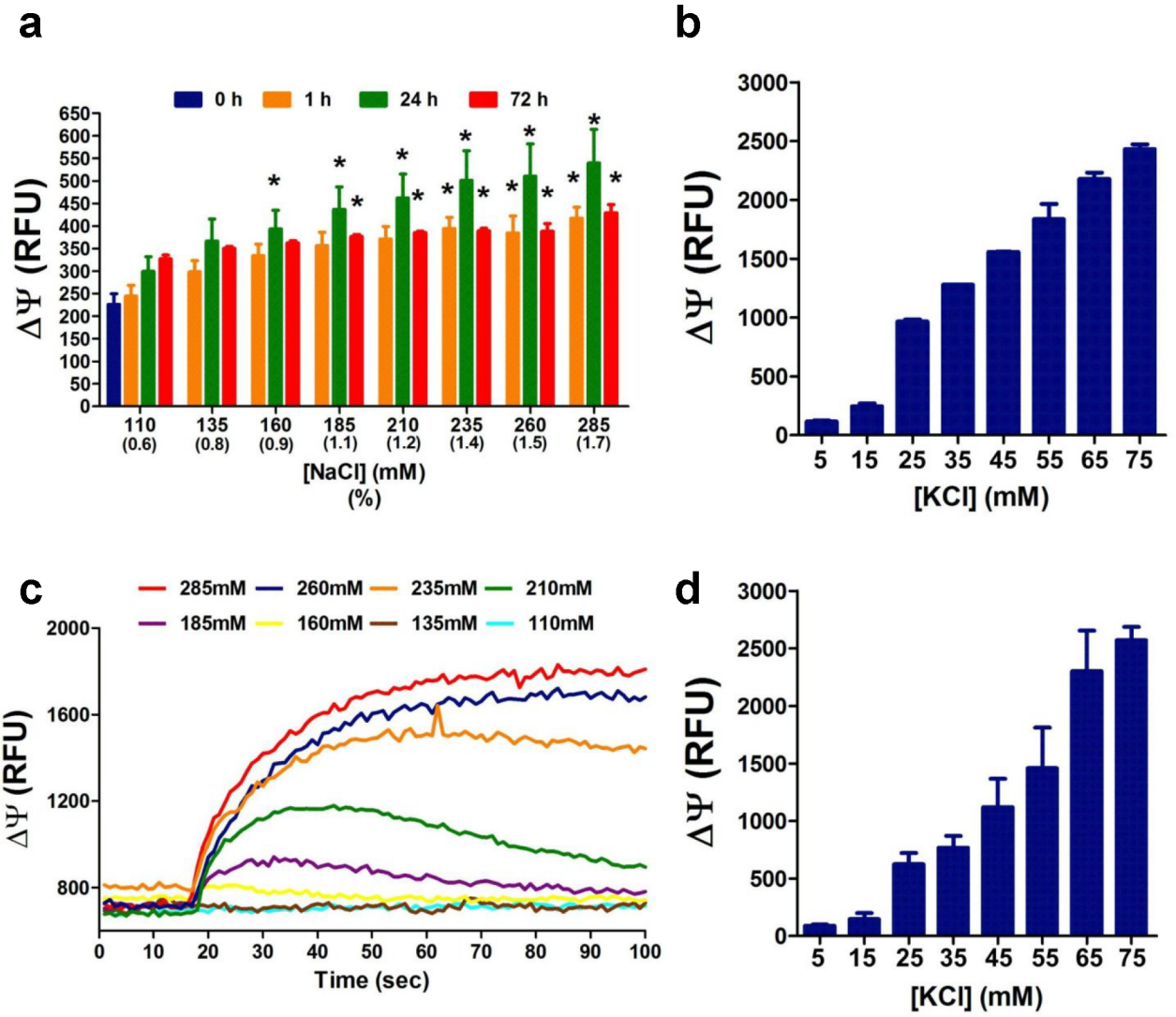

Figure 3. Vero and Calu-3 cell membrane depolarization by increasing concentrations of NaCl and KCl. (a) Membrane potential indicated as relative fluorescence units (RFU) in Vero cells after 0, 1, 24, and 72 h post-treatment with increasing concentrations of NaCl (110 up to 285 mM) as determined by microfluorimetry. Increasing NaCl concentration caused membrane depolarization that was maximal after 24 h and tended to return to control values after 72 h of treatment. (b) Increasing KCl concentrations caused immediate membrane depolarization at concentrations above 25 mM in Vero cells as determined by real time fluorescence measurements. (c) The increasing NaCl concentrations caused an immediate membrane depolarization at concentrations above 160 mM. Membrane depolarization of cells treated with up to 210 mM NaCl returned to the resting point after 70 s. (d) Increasing KCl concentrations caused immediate membrane depolarization at concentrations above 25 mM in Calu-3 cells as determined by real time fluorescence measurements. Data are representative of three independent experiments and shown as mean values ± SEM; one-way ANOVA (*$p < 0.05$).

containing increasing concentrations of NaCl for 1 h before absorption. Such treatment (pre-exposure) with NaCl did not affect viral replication at any tested concentration (Figure 1a, VPI curve). The same result was observed when we treated cells with NaCl 1 h before infection (Figure 1a, AD curve). On the other hand, significant inhibition of viral replication (up to 50%) was seen when as little as 160 mM of NaCl was available during virus replication alone (Figure 1a, $p = 0.032$, PI curve) or full-time, during adsorption and replication (Figure 1a, $p = 0.030$, FT curve). There was not any statistically significant difference between postinfection (PI) and adsorption plus postinfection (FT) treatments ($p = 0.985$). Altogether, these data suggest that SARS-CoV-2 inhibition in the presence of NaCl reflects an intracellular mechanism and is not ascribed to the dissociation of Spike SARS-CoV-2 and human ACE-2 protein complexes.

The antiviral activity of NaCl was not caused by cytotoxic effects of NaCl on Vero cells, as determined by the AlamarBlue Cell Viability Reagent (Figure 1b) and LDH assays (Figure 1c). Furthermore, we determined cell death rates to confirm the integrity of cells after being exposed to NaCl in the same conditions performed in the experiments performed in the presence of the virus. We observed less than 8% cell death at all tested NaCl concentrations (Figure 1d). We observed less than 20% cytotoxicity (cell viability above 80%) at all tested NaCl concentrations (Figures 1b, c, and d). SARS-CoV-infected and noninfected Vero cells were analyzed by an indirect immunofluorescence assay, and NaCl concentrations greater than 185 mM NaCl (1.1%) significantly inhibited virus replication without appreciably affecting cell viability (Figure 1e).

https://doi.org/10.1021/acsptsci.1c00080
ACS Pharmacol. Transl. Sci. XXXX, XXX, XXX−XXX

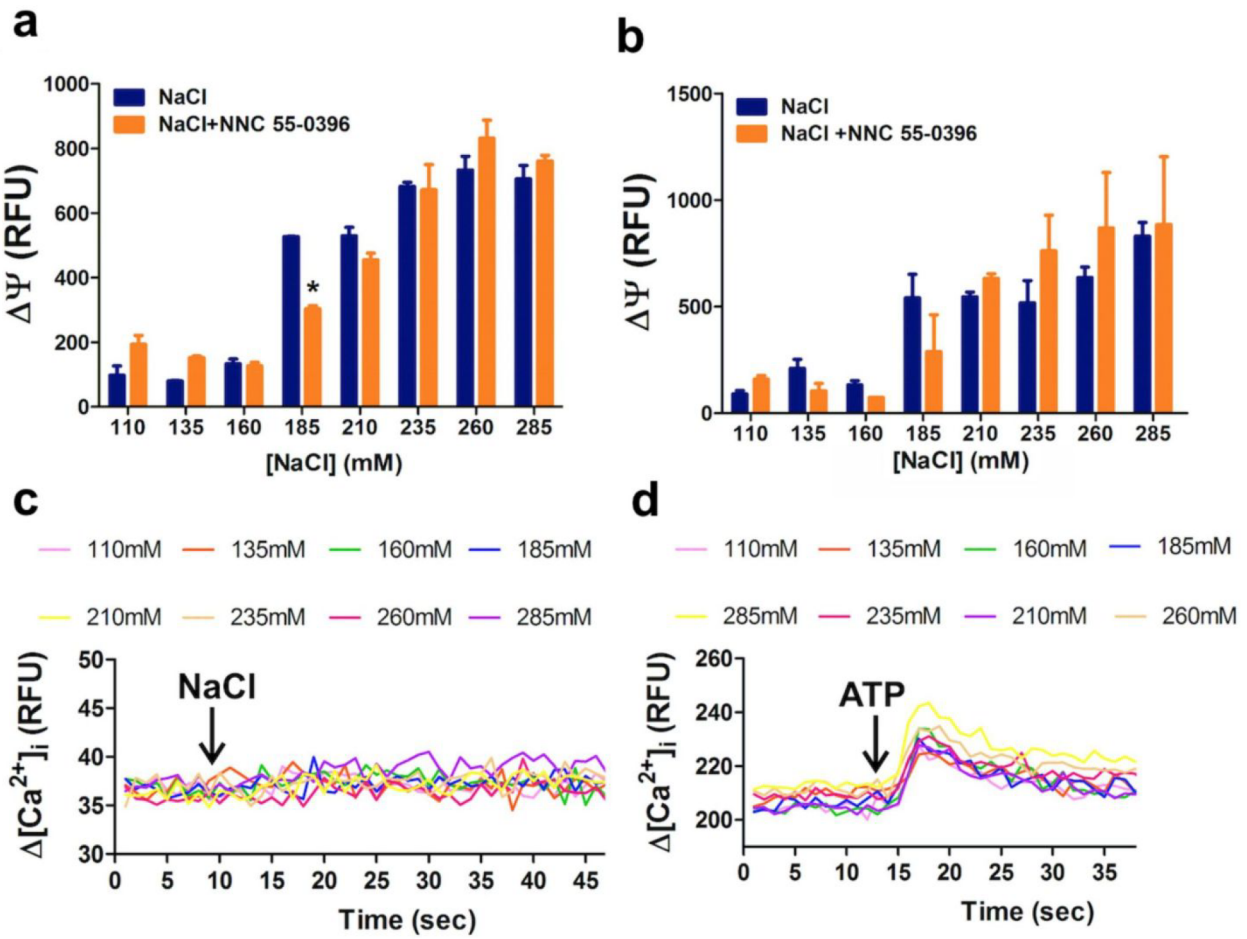

Figure 4. Increasing concentrations of NaCl affect ATP homeostasis independently of voltage-gated calcium channels. Membrane potential indicated as relative fluorescence units (RFU) in Vero cells (a) and Calu-3 cells (b) 3 min after the addition of increasing concentrations of NaCl (110 up to 285 mM) as determined by microfluorimetry. NN55-0396 (1 μM), a blocker of Cav Ca^{2+} channels, was incubated 5 min prior to NaCl challenge. (c, d) Variations in intracellular free calcium $[Ca^{2+}]_i$ concentration, indicated as relative fluorescence units (RFU) in Vero cells exposed to increasing concentrations of NaCl (110 up to 285 mM) (c) and upon addition of 10 μM ATP (shown by arrows) (d), as determined by microfluorimetry. The data are representative of three independent experiments and shown as mean values ± SEM; two-way ANOVA ($*p \leq 0.05$).

Hypertonic Saline Solution Inhibits SARS-CoV-2 Replication in Human Lung Epithelial Cells. We further evaluated if a similar inhibition profile of NaCl in SARS-CoV-2 replication could be observed in a human Calu-3 (ATCC HTB-55) lung cell line that has shown to be susceptible to SARS-CoV-2.[19] First, we noticed a greater cytotoxicity of NaCl in this cell type (more than 30% cell death), when compared with Vero cells. However, there was a significant reduction of viral replication at 185 mM NaCl (Figure 2a line green, 88% reduction, $p < 0.001$) and 210 mM NaCl (Figure 2a line green, 90% reduction, $p < 0.001$). These concentrations of NaCl were not cytotoxic (cell viability above 70%) for Calu-3 cells (Figure 2a, orange line).

Even with different NaCl tolerances and inhibition potencies of viral replication between Calu-3 and Vero cells, these data are relevant with up to 90% inhibition of virus replication at non-toxic NaCl concentrations. A recent work highlighted the fact that cell lines mimicking important aspects of respiratory epithelial cells should be used when analyzing the antiviral activity of compounds that target host cell functions.[20]

Hypertonic Saline Solution Causes Cell Membrane Depolarization in NaCl Dose-Dependent Manner. In order to determine whether hyperosmotic stress would cause membrane depolarization, Vero cells were incubated with different NaCl concentrations (135, 160, 185, 210, 235, 260, and 285 mM equivalent to 0.8, 0.9, 1.1, 1.2, 1.4, 1.5, and 1.7%, respectively), and assayed following 1, 24, and 72 h of incubation (Figure 3a). Results are indicated as relative fluorescence units (RFU), whose increased values refer to membrane depolarization. Cells showed a rapid membrane depolarization effect upon stimulation with increasing NaCl concentrations (Figure 3b). The membrane depolarization effect was dose-dependent, with statistical differences starting at 160 mM NaCl. Results obtained 24 h after incubation with NaCl showed that the depolarization of the membrane increased with the time of exposure. The membrane potential tended to return to control values 72 h after exposure to NaCl, indicating that Vero cells were partially capable of recovering their resting membrane potential.

The SARS-CoV-2 inhibition assays were performed using monkey kidney cells that, similarly to lung epithelial cells, are heavily infected by SARS-CoV-2[19,21] and perform endo- and exocytosis, therefore being a good cell line model to study the SARS-CoV-2 life cycle. Our results show that an increase of NaCl as well as KCl concentrations causes immediate membrane depolarization of Vero and Calu-3 cells (Figure

https://doi.org/10.1021/acsptsci.1c00080
ACS Pharmacol. Transl. Sci. XXXX, XXX, XXX−XXX

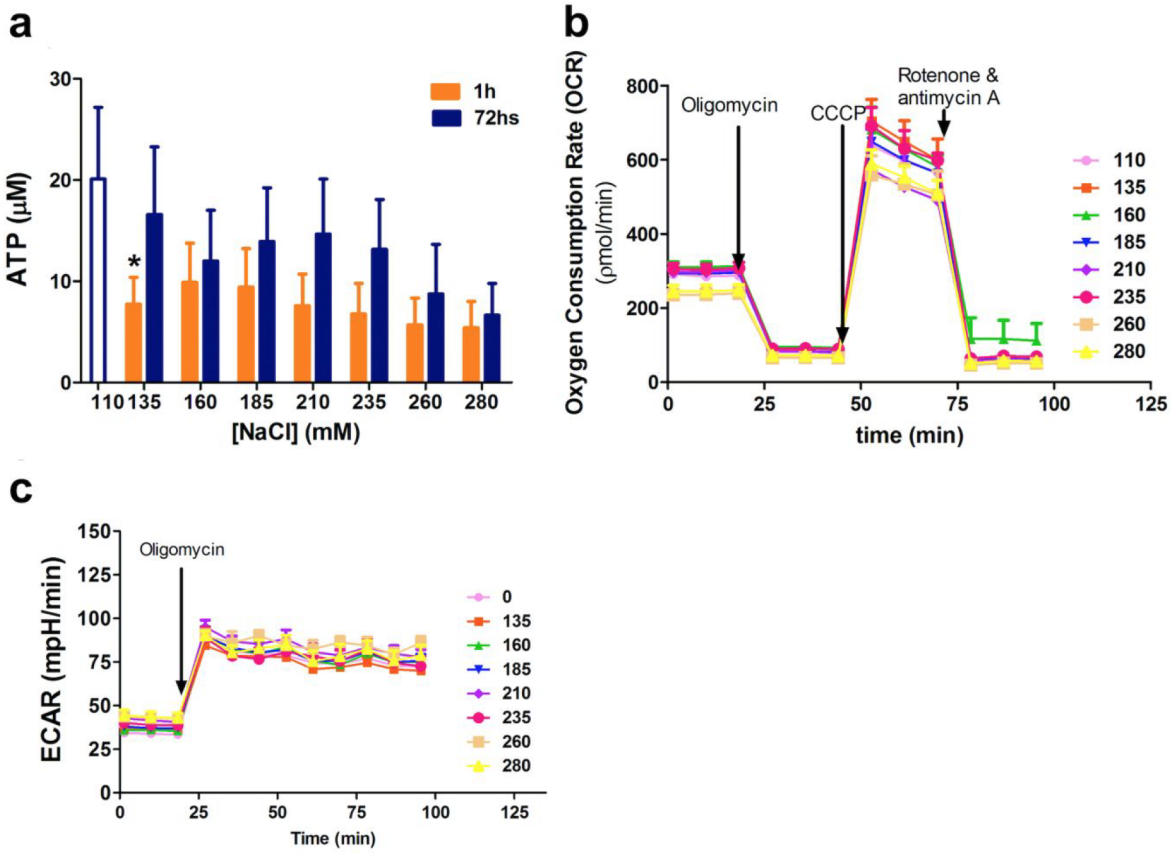

Figure 5. NaCl-induced depolarization affects the cell energetic state without impairment of mitochondrial function. (a) Total cellular ATP quantification of Vero cells treated for 1 h or 72 h with increasing NaCl concentrations by the luciferase assay. The oxygen consumption rate, OCR, (b) and the extracellular acidification rate, ECAR, (c) were measured in cultured Vero cells (40 000 cells/well) after 72 h of NaCl incubation, using Seahorse technology with the Mito Stress Test kit. Sequential injections of oligomycin, carbonyl cyanide 3-chlorophenylhydrazone (CCCP), and rotenone plus antimycin A are indicated. Mitochondrial respiration was evaluated under four different conditions: *basal respiration*, corresponding to the cell basal consumed oxygen; *proton leak*, after oligomycin (ATP-synthase blocker) addition; *uncoupled*, after addition of the respiratory chain uncoupler CCCP, where the oxygen consumed reflects the maximal respiration rate (irreversibly uncoupling from ATP synthesis); and *inhibited*, through complex I and complex III total inhibition by rotenone and antimycin A, respectively. The ECAR rate was verified by application of the glycolysis stress test kit (Agilent Technologies). The data are representative of three independent experiments and shown as mean values ± SEM; two-way ANOVA ($*p \leq 0.05$).

3c and d), probably through the activation of an extracellular Na^+ sensitive channel, called Na_x.[22]

Voltage Gated Ca^{2+} Channels Do Not Participate in Hypertonic Saline Solution-Induced Membrane Potential Impairment in Both Vero and Calu-3 Cell Lines. In order to understand the mechanism involved in virus inhibition by NaCl, we performed membrane potential assays that show a direct relationship between NaCl concentration and membrane depolarization. The activation of Na_x channels, highly expressed in epithelial cells,[23] supposedly leads to Na^+ inward flow, causing depolarization, which in turn might activate Cav2.1 voltage-gated Ca^{2+} channels that are expressed at the apical membrane of epithelial cells.[23]

Voltage-gated calcium channel activity is known to be involved in cell viral infection. In Vero cells, the application of T-type Ca^{2+} channel selective blockers inhibited infection by Herpes simplex virus type 2 (HSV-2), which did not occur for voltage-gated L-type Ca^{2+} channels.[23,24] Inhibition of T-type Ca^{2+} channel activity by NNC 55-0396[25] did not affect membrane potential at most NaCl concentrations, indicating that this voltage-gated channel is not involved in the depolarization observed in Vero and Calu-3 cells (Figure 4a and b). Since there are several other types of voltage-gated Ca^{2+} channels, we sought to evaluate if NaCl-induced depolarization promoted calcium transients in Vero cells in the first place (Figure 4c). In agreement with our results, calcium influx was not noted under the present conditions of hypertonic NaCl solutions. ATP (10 μM)-induced $[Ca^{2+}]_i$ transients provided a positive control for confirming Vero cell viability and responsiveness of the intracellular calcium signaling system (Figure 4d). Thus, we conclude that calcium is not involved in NaCl-promoted effects. This may also indicate that potassium channels activated by calcium, such as small conductance (SK) and big conductance (BK) channels,[25,26] are also not involved in NaCl-induced depolarization and following repolarization to resting potential conditions.

Energy Balance (ATP/ADP) As a Central Mechanism for Virus Replication Inhibition Induced by Hypertonic Saline. An important influence on viral replication is the amount of ATP available, once viral processes require a robust energy expenditure.[27] Therefore, we measured with the luciferase assay the total intracellular ATP levels in Vero cells treated for 1 h or 72 h with hypertonic solutions of NaCl. The indirect method of relative ATP concentration quantification by luciferase activity showed significantly lower levels of ATP

https://doi.org/10.1021/acsptsci.1c00080
ACS Pharmacol. Transl. Sci. XXXX, XXX, XXX−XXX

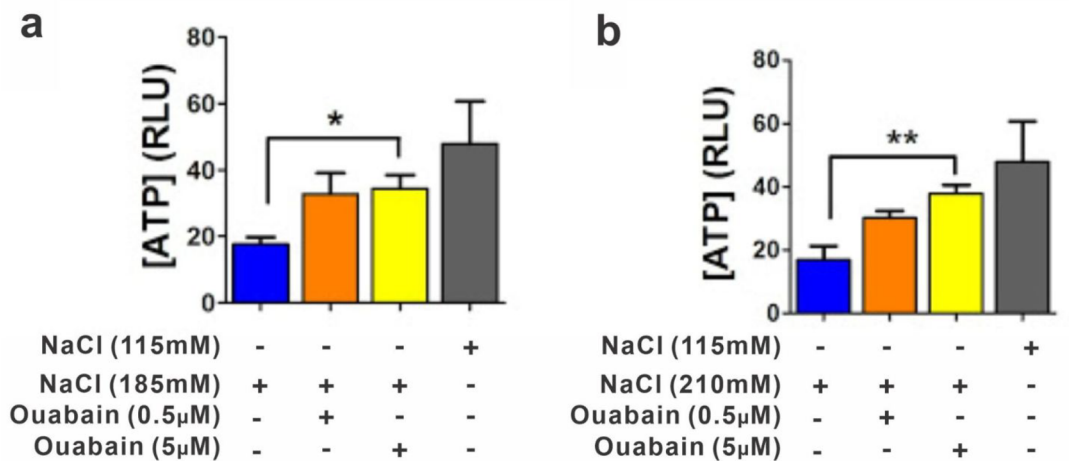

Figure 6. Ouabain treatment abolished the cell energetic state impairment caused by NaCl. Relative quantification of cellular ATP concentrations of Vero cells treated for 1 h with DMEM cell culture medium, containing 115 mM NaCl (resting conditions) or with DMEM with NaCl supplemented to 185 or to 210 mM final NaCl concentrations, as shown in panels a and b, respectively. Relative ATP concentrations were measured by a luciferase assay. The data are representative of three independent experiments and shown as mean values ± SEM; one-way ANOVA ($^*p \leq 0.05$, $^{**}p \leq 0.01$).

following 1 h versus 72 h of inhibition (Figure 5a), at depolarized and resting membrane potential, respectively.

We hypothesized that hyperosmotic stress would result in impaired mitochondrial function, affecting the production of ATP, thus inhibiting virus replication. Also, it is known that mitochondrial depolarization may lead to cell membrane depolarization,[28] which would explain the effect observed with NaCl incubation. To determine if NaCl addition was causing mitochondrial disruption, mitochondrial metabolism of intact Vero cells was assessed with a high-resolution respirometry assay. For this, two parameters were evaluated: oxygen consumption rate (OCR; Figure 5b) and extracellular acidification rate (ECAR; Figure 5c). When mitochondrial metabolism is compromised, glycolytic enzymes enhance their activity to compensate for ATP production. The end product of this pathway is lactate, and its synthesis and accumulation results in medium acidification.[29] Figure 5b shows oxygen consumption in four states: basal, proton leak, uncoupled, and inhibited (see methods). *Basal* indicates normal cell respiration values; *proton leak* reflects mitochondrial inner membrane integrity; *uncoupled* indicates respiratory chain activity of complex I to IV (i.e., maximal respiratory capacity); and *inhibited* reflects nonmitochondrial processes that consume oxygen. After 72 h of NaCl addition in cultured Vero cells, there was no difference compared to control values. In agreement, ECAR evaluation (Figure 5c) indicated that NaCl addition, in all concentrations, was not enough to shift the metabolism to the anaerobic pathway, as a compensation to maintain cell basal ATP levels. OCR and ECAR results indicate that all tested NaCl concentrations did not impair mitochondrial function in Vero cells. For any studies of chemicals with therapeutic potential, such a result is important since it is common to observe mitochondrial impairment during the development of new drugs.[30] Therefore, inhibition of SARS-CoV-2 replication in Vero cells by hypertonic solution is not due to mitochondrial membrane depolarization, but it is due to the exacerbated consumption of ATP necessary for re-establishing the resting membrane potential.

Na^+/K^+ ATPase Is the Main Pump for Depleting the ATP Stock of the Cells in Order to Recover the Resting Membrane Potential. We observed that NaCl-caused ATP intracellular energy depletion was not due to a mitochondrial dysfunction (Figure 5). In view of that, we hypothesized that a decrease of intracellular ATP levels may be due to over-stimulation of the Na^+/K^+ ATPase pump. In order to test this hypothesis, we inhibited the Na^+/K^+ ATPase pump using ouabain to observe if the effect in ATP is reversed if ATP depletion would be reversed. We performed assays using Vero cells in the presence of 185 and 210 mM NaCl in the presence and absence of ouabain (0.5 μM and 5 μM). In the presence of ouabain, blocking the activity of Na^+/K^+ ATPase, no statistically significant decay of intracellular ATP concentration at 185 mM and 210 mM NaCl is seen, as shown in Figure 6a and b, respectively. Therefore, Na^+/K^+ ATPase is the main pump depleting the ATP stock of the cells in order to recover the resting membrane potential.

DISCUSSION

Vesicle formation is important for kidney and lung cells as responses to alteration of osmosis, regulated by aquaporin channels,[31] as well as for vesicle transfer between cells, which has been suggested to contribute to lung disease and possibly to the propagation of the SARS-CoV-2 virus into neighboring cells.[31,32] Following that line, a hyperosmotic response by high extracellular salt concentration may influence the functionality of different membrane channels, which could affect endocytosis and, thereby, decrease the efficiency of entrance of SARS-CoV-2 into cells. Endocytic, clathrin-independent, lipid-raft involving virus entry has been described for SARS-CoV,[33] supporting a role of endocytosis in SARS-CoV-2 cell entry.

During SARS-CoV-2 infection, pulmonary edema and cytokine storms are responsible for the most lethal scenarios.[33,34] The increased amount of liquid blocking the airway at the alveoli causes extreme injury, and fibrotic scar tissue substitutes the injured tissue (Figure 7a). Along with embryonic pulmonary development, the organ is full of liquid, which is removed mainly by the action of sodium channels, such as epithelial sodium (Na^+) channels (ENaCs) that are sensitive to amiloride.[22,35−37] These ENaCs are expressed mainly by epithelial cells of different organs, such as kidneys, lungs, colon, skin, and by some neurons in the brain.[22] In

https://doi.org/10.1021/acsptsci.1c00080
ACS Pharmacol. Transl. Sci. XXXX, XXX, XXX−XXX

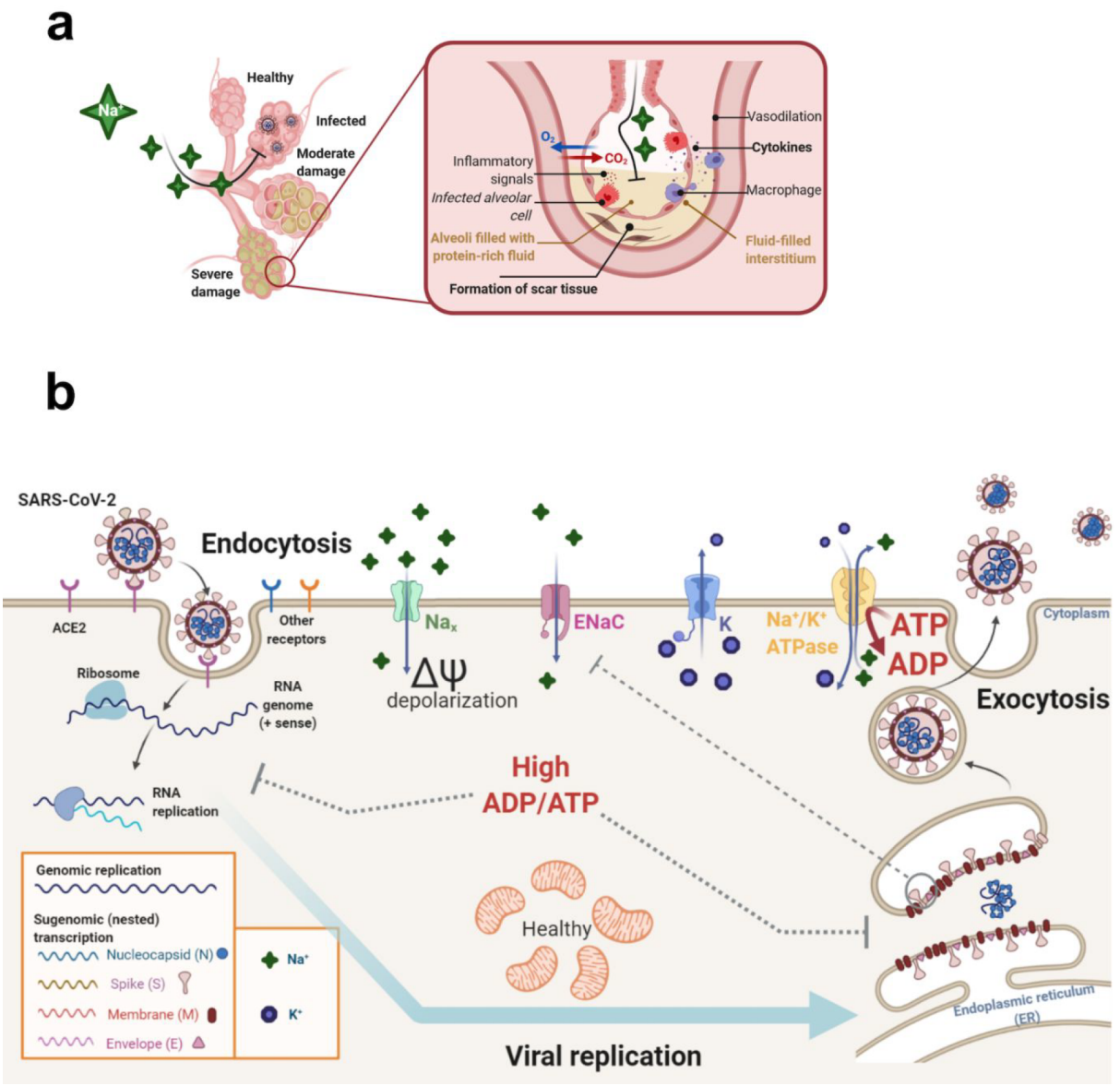

Figure 7. Confirmed and suggested mechanisms of NaCl hyperosmotic treatment resulting in SARS-CoV-2 replication inhibition. (a) Illustration of SARS-CoV-2 alveoli infection, which can lead to pulmonary edema, high levels of cytokines, and tissue damage. (b) Hypothesis for a possible mechanism involving the effect of NaCl treatment in the inhibition of SARS-CoV-2 replication in Vero and Calu-3 cells. Hypertonic saline solution causes membrane depolarization and an overflow of Na^+ in cells, causing a low energy state (high ADP/ATP concentration ratio), leading to impaired virus replication. Hyperosmotic extracellular NaCl concentrations probably activate sodium-sensitive (but not voltage-sensitive) Na_x channels, which are critically involved in body-fluid homeostasis. High cytoplasmic Na^+ concentrations can recruit epithelial sodium (Na^+) channels (ENaC), further increasing intracellular Na^+ concentration, causing cell membranes to depolarize. The activation of K^+ channels may also happen to pump out K^+. Na^+/K^+ ATPase activation for restoring resting membrane potential results in increased ADP/ATP ratio. This low energetic state would be detrimental for viral replication. Thus, the imbalance of intracellular K^+ concentration may also affect the functioning of different potassium channels that may be important for the virus life cycle. The illustration was created with the web-based tool BioRender (https://biorender.com).

adulthood, ENaC usually controls the concentration of Na^+ in the extracellular environment. Therefore, the channels are extremely important for the organism's water balance, by controlling reabsorption of Na^+ in kidneys, sweat, and the colon. In this way, the activity of ENaC can influence blood pressure and the renin-angiotensin system, as well as the thickness and dryness of the airway.[22] Interestingly, this channel is also involved in taste sensation, and its improper functioning could be related to a loss of taste.[22]

Our data show the efficiency of hypertonic NaCl solutions in blocking SARS-CoV-2 replication in Vero monkey kidney epithelial cells as well as in Calu-3 human lung epithelial cells. These data suggest that hypertonic solutions could be investigated as a prophylaxis or an alternative treatment for COVID-19 patients. The data regarding the membrane potential, obtained by us, point to a possible inhibition mechanism of SARS-CoV-2 infection in Vero and Calu-3 cells by extracellular increased concentration of NaCl. Various pulmonary virus infections impair the activity of ENaC, and the increased activation state of these channels can significantly decrease influenza A infection.[38−40] Additionally, the spike (S) and envelope small membrane proteins (E) of SARS-CoV can

https://doi.org/10.1021/acsptsci.1c00080
ACS Pharmacol. Transl. Sci. XXXX, XXX, XXX−XXX

directly decrease the inward current of ENaC as well as decrease its expression through the protein kinase C (PKC) signaling pathway.[22] Impairment of ENac activity itself would be enough to explain pulmonary edema in the alveoli, since its inhibition would increase the amount of Na^+ in the airway, and water would flow by osmosis.[22,41]

Moreover, the sodium-concentration ($[Na^+]$)-sensitive Na channel (Na_x) is a sodium sensor that controls salt-intake behavior.[42] Its activation upregulates prostasin (protease) release into the extracellular space, activating ENaC by cleaving the extracellular loop of the γ ENaC subunit.[43−45] Following Na^+ influx via ENaC, the cells also present downstream mRNA synthesis elevation of inflammatory mediators.[45] In the same line, Na_x expression blockade can improve scarring.[45] Therefore, an extracellular Na^+ imbalance through ENac inefficiency by SARS-CoV-2 infection may explain the formation of pulmonary fibrosis due to virus infection.

The membrane potential has been shown to be important for cell infection by some viruses, as in the case of human rhinovirus type 2 infection, in which membrane hyperpolarization enhances infection.[46] Inhibition of membrane depolarization is part of the viral lung infection strategy, as shown for SARS-CoV[22,46] and respiratory syncytial virus,[22,46,47] whose cell infection inhibits the entry of Na^+ into the cell. While the ENac is voltage-insensitive, the gradient between high and low Na^+ (outside and inside of the cell) would force the entry of Na^+, being an unfavorable condition for SARS-CoV-2 infection, which may explain virus replication inhibition by NaCl.

We also observed that NaCl causes ATP intracellular energy depletion. In view of that, we tested the hypothesis that mitochondrial dysfunction was contributing to the antiviral effect, as mitochondrial membrane potential can be determinant for antiviral cell responses. In human embryonic kidney (HEK) and mouse embryonic kidney (MEF) cells, the application of the mitochondrial uncoupler carbonyl cyanide 3-chlorophenylhydrazone (CCCP), which dissipates the transmembrane potential through the increase of membrane permeability, impaired the antiviral response of the cell.[48] This did not occur in the presence of the F_1F_O ATP synthase inhibitor oligomycin B, indicating that the observed diminished antiviral effects were associated with mitochondrial membrane depolarization, but not with impaired ATP synthesis alone. In our work, oxygen consumption results indicate that, in Vero cells, the addition of NaCl did not compromise mitochondrial metabolism (Figure 5b and c). These results are promising, as viral replication impairment was not accompanied by cytotoxicity. The importance of mitochondrial function in human health is clear, when impacts of mutations on mitochondrial DNA or nuclear proteins critical for mitochondria activity are evaluated. In such cases, the respiratory as well as peripheral and central nervous systems, heart, liver, skeletal muscle, and kidneys, are affected.[49] In addition, mitochondrial impairment is considered to be a major contributor for the development of cardiac and hepatic toxicity induced by drugs, such as cerivastatin, troglitazone, and tolcapone.[30] Thus, the results indicating that increasing NaCl concentrations does not disrupt mitochondrial metabolism is a positive outcome for future clinical trials.

We observed mainly two patterns of depolarization: (1) lower concentrations of NaCl triggered depolarization, and after 180 s the cell membrane reestablished the resting state, causing a timid inhibition of the virus release, while (2) concentrations higher than 210 mM could trigger a high amplitude depolarization, in which the cells needed periods longer than 24 h to recover the resting state, causing over 90% inhibition of virus replication (Figures 1a and 2b). Based on our results that show NaCl dose-dependent SARS-CoV-2 replication inhibition, membrane depolarization and intracellular ATP stock depletion, we propose the following mechanism (Figure 7b): In the first situation, we hypothesize that activation of K^+ channels and Na^+/K^+ ATPase pumps could recover the steady state in the short term, while in the second situation, the over stimulation of Na_x and ENaC would overwhelm the cell by prolonged activation of the Na^+/K^+ ATPase pump, consuming cellular ATP, thus resulting in low ATP stores. Our data indicate that cytosolic ATP concentration decreases with prolonged depolarization mainly induced by NaCl incubation for 1 h, corroborating the hypothesis that virus replication inhibition depends on the availability of host energy.

Hypertonic nasal saline, which facilitates mucociliary clearance, may have an important role in SARS-CoV-2, since it is a highly virulent respiratory virus with significant presence in the nasal and nasopharyngeal mucosa.[50] Our data shows that NaCl decreases viral replication by more than 90%, probably due to a mechanism associated with the effect of membrane depolarization and consequently a high ADP over ATP concentration ratio. Since Na_x and ENaC channels face the luminal surface (air space), they will be the sensors of higher concentration of salt in the alveoli. Basolateral Na^+/K^+ ATPase would transport the Na^+ from inside of the epithelial cells to the interstitial space that connects to capillaries. Consequently, Na^+ would be diluted by the blood flow.[45] Therefore, a possible treatment with hypertonic saline solution (1.1−1.4% NaCl) probably will have a local effect of inhibiting virus replication. This low salt amount is not expected to cause any systemic hypertension in the organism.

Besides the mechanism we have investigated, there is also an immune approach that could investigate the release of pro- or anti-inflammatory cytokines. The literature already reported inhibitory effects on IL-6 and IL-8 release and in respiratory syncytial virus infection by hypertonic saline solution treatment in cultures of human respiratory epithelial lines.[51] However, our *in vitro* model has some limitations to resemble the lung, since it does not contemplate the immune system. It would be interesting to further investigate the role of hypertonic saline solution treatment in macrophages as well, since elevated concentrations of NaCl enhance the conversion of Cl^- and hydrogen peroxide (H_2O_2) to hypochlorous acid (HOCl) in nonmyeloid cells.[17,52] HOCl has septic properties that would locally shield the tissue, preventing virus infection.

It is worth mentioning that hypertonic solution treatment is used to improve lung function in cystic fibrosis patients.[53] Moreover, nebulized 3% hypertonic saline treatment for infants with moderate to severe bronchiolitis is safe without any adverse events, such as bronchospasm, cough, or wheezing aggravation.[54−56] Furthermore, a posthoc analysis of NCT02438579 clinical trial suggests that hypertonic saline nasal irrigation and gargling may have played a role in reducing symptoms and duration of illness caused by COVID-19.[57] In addition, given available evidence, the scientific community has been proposing that saline irrigations with or without indicated additives may be safe for use in COVID-19 patients.[58,59] In

https://doi.org/10.1021/acsptsci.1c00080
ACS Pharmacol. Transl. Sci. XXXX, XXX, XXX−XXX

that way, there are three clinical trials registered in ongoing status (NCT04465604, NCT04382131, and NCT04341688) according to ClinicalTrials.gov (https://clinicaltrials.gov/ct2/home), related to the use of hypertonic saline solution for COVID-19 treatment. This scenario highlights the importance of our results and reinforces the need of carrying out clinical studies for a better understanding of the benefits of hypertonic saline treatment for COVID-19 patients.[59]

In summary, hypertonic saline solution inhibits SARS-CoV-2 virus replication in Vero monkey epithelial kidney cells and Calu-3 human lung epithelial cells due to perturbation of one or several steps of the virus intracellular life cycle. Our results suggest that more than 185 mM NaCl (1.1%) causes membrane depolarization resulting in insufficient ATP stocks available for virus replication, therefore being a general mechanism to avoid virus replication inside cells *in vitro* assays. Hence, the complete molecular mechanism underlying the observed phenomenon may be more complex, involving several factors that together result in the inhibition of viral infection. Nevertheless, we highlight that *in vivo* experiments and clinical trials should be carried out in order to prove the efficacy of hypertonic saline treatment in humans with COVID-19.

EXPERIMENTAL SECTION

Cell, Virus, and NaCl Dilution. The African green monkey kidney Vero E6 cell line (ATCC CCL-81) and human lung epithelial cell line Calu-3 (ATCC HTB-55) were maintained in Dulbecco's modified eagle medium (DMEM), supplemented with 10% fetal bovine serum (FBS), 1% nonessential amino acids (NEAA), 1% sodium pyruvate (Sigma-Aldrich Co., Deisenhofen, Germany), and incubated in a humidified atmosphere containing 5% CO_2 at 37 °C. A clinical isolate of SARS-CoV-2/SP02/human/2020/BRA (GenBank access no. MT126808.1) was propagated in Vero cells, and the viral titer was determined by 50% tissue culture infective dose ($TCID_{50}$) and by plaque forming units per milliliter (PFU/mL), as previously described by Araujo and collaborators.[60] We conducted all infection experiments in a biosafety level-3 (BLS-3) laboratory at the Institute of Biomedical Sciences, University of São Paulo, São Paulo, Brazil, following the Laboratory biosafety guidance related to the novel coronavirus (2019-nCoV) by the WHO.[61] Sodium chloride (NaCl) was diluted in free-DMEM that already contains in its composition 110 mM NaCl. In that way, we assumed seven additional increased concentrations (25, 50, 75, 100, 125, 150, and 175 mM) of NaCl in the cell medium, resulting in final NaCl concentrations of 135, 160, 185, 210, 235, 260, and 285 mM.

Antiviral Activity of NaCl during Different Times of Addition. Vero cells were seeded in a clear-bottom 96-well plate (5×10^4 cells/mL) and incubated for 24 h at 37 °C for cell adherence. Then, they were treated with increasing concentrations of NaCl at different stages of virus infection as described below. Four different NaCl times of addition were evaluated,[16,62] compromising virus preincubation (VPI), absorption (AD), postinfection (PI), and adsorption plus postinfection, named full-time (FT). For the VPI treatment, SARS-CoV-2 was preincubated with increasing concentrations of NaCl for 1 h before infecting the cells. After adsorption, the inoculum was removed, replaced with media, and maintained until the end of the experiment. For AD treatment, the different concentrations of NaCl were added to the cell monolayer for 1 h prior to virus infection and maintained for 1 h for the viral attachment process. Then, the virus−NaCl mixture was replaced with fresh DMEM until the end of the experiments. During the PI-staining experiment, the virus was added to the cells to allow infection for 1 h, and then the virus-containing supernatant was replaced with a different NaCl-concentration-containing medium until the end of the experiment. For FT treatment, Vero cells were pretreated with different concentrations of NaCl for 1 h prior to virus infection, followed by incubation with the virus for 1 h in the presence of the NaCl. Then, the virus mixture was removed, and cells were cultured with the same concentrations of NaCl-containing medium until the end of the experiment. For all experimental groups, cells were infected with the virus at a multiplicity of infection (MOI) of 0.02, and at 72 h postinfection (h.p.i.). Then, cell supernatants were collected for RT-qPCR, and cells were screened for the presence/absence of cytopathic effects (CPE) under an optical microscope (Olympus, Tokyo, Japan).

Nucleic Acid Extraction and Quantitative Real-Time RT-PCR (RT-qPCR). In order to perform the quantification of SARS-CoV-2 viral load, the extraction of total nucleic acid (RNA and DNA) from the collected cell culture supernatant was carried out, using the semiautomated NucliSENS easyMag platform (BioMerieux, Lyon, France), following the manufacturer's instructions. The quantification of viral RNA was done using the AgPath-ID One-Step RT-PCR Kit (Applied Biosystems, Weiterstadt, Germany) on an ABI 7500 SDS real-time PCR machine (Applied Biosystems) using a reference published sequence of primers and probe for the E gene.[63] Numbers of RNA copies/mL were quantified using a specific in vitro-transcribed RNA quantification standard, kindly granted by Christian Drosten, Charité - Universitätsmedizin Berlin, Germany, as described previously.[64]

Indirect Immunofluorescence (IFI). The methodology here described for determination of the number of active SARS-CoV-2 viruses was adapted from Sales-Medina et al.[65] Briefly, after 72 h.p.i, the plates were fixed for 30 min in 4% paraformaldehyde in 1× PBS (pH 7.4) and subjected to indirect immunofluorescence detection of viral cellular infection. After washing twice with 1× PBS, containing 0.05% Tween 20 (PBST), plates were blocked with bovine serum albumin (BSA; 5% w/v in 1× PBS; Sigma-Aldrich) for 30 min at room temperature and washed twice with PBST. As a primary antibody, we used serum from a COVID-19 convalescent Brazilian patient diluted 1:1000 in PBS to detect SARS-CoV-2 infection in Vero cells. The primary antibodies were incubated for 30 min, and plates were washed twice with PBST. As secondary antibodies, goat antihuman IgG labeled with Alexa 488 (Thermo Scientific) was used, diluted at 4 μg/mL in PBS and incubated for 30 min with 5 μg/mL 4′,6-diamidino-2′-phenylindole dihydrochloride (DAPI, Sigma-Aldrich) in PBS to stain nucleic acid. The plates were washed twice with PBST and imaged in the Operetta High Content Imaging System (PerkinElmer) using a 20× magnification objective. Five images were acquired per well and analyzed in the software Harmony (PerkinElmer), version 3.5.2. Image analysis consisted of identifying and counting Vero cells based on nuclear segmentation and viral infection based on cytoplasmic staining detected by the immunofluorescence assay.

Cell Viability Assays. For determination of Vero and Calu-3 cell viability and stress, 5×10^4 cells adhered to black

https://doi.org/10.1021/acsptsci.1c00080
ACS Pharmacol. Transl. Sci. XXXX, XXX, XXX−XXX

clear-bottom 96 well plates and were stained with the AlamarBlue Cell Viability Reagent (Thermo Fisher Scientific), according to the manufacturer's instructions. Fluorescence intensities were recorded at rest (point 0 h), 1 h, 24 h, and 72 h after NaCl challenge, using 530 nm for excitation and 560/590 for emission detection in the FlexStation III microplate reader (Molecular Devices, Sunnyvalley, CA). Data were normalized with a blank control that consists of cell medium for natural reduction conditions. Data are plotted as a reference to the basal condition of 110 mM NaCl concentration (DMEM's salt concentration). Cell viability was further evaluated using a colorimetric assay by quantifying lactate dehydrogenase (LDH) released into the culture supernatant from cells with damaged membranes, using the CytoTox 96 Non-Radioactive Cytotoxicity Assay (Promega Corp., Madison, WI). Detection was performed using a microplate reader (POLARstar Omega, BMG LABTECH, Ortenberg, Germany) at 492 nm. The activity of the released LDH was reported as a percentage of the total cellular LDH (measured after the complete lysis of control cells corresponding to the maximal amount that can be released by cells, therefore 100%). Cell viability was normalized to that of untreated cells (no NaCl added). A viability of 70% was used as a threshold for cytotoxicity.[66]

Cell Death Quantification. For cell death detection, we adapted a usual method for flow cytometry, based on staining live cells with the cell membrane-impermeant dye, propidium iodide (PI), and the cell membrane-permeable fluorophore, Hoechst 33342. Since PI stains dead cells, while Hoechst 33342 stains every cell in the dish, cell death rates were quantified by the total fluorescence intensity of the PI staining in the well, normalized by the total fluorescence intensity of Hoechst 33342.[67] The recordings were acquired at rest (point 0 h), 1 h, 24 h, and 72 h after NaCl challenge, using 535 nm for excitation and 617 nm for emission to detect PI and 350 nm for excitation and 461 nm for emission of Hoechst 33342 in the FlexStation III microplate reader. For positive controls of total cell death, cells were lysed with 1% TritonX-100 detergent.

Analysis of Membrane Potential Variation by Microfluorimetry. Changes of the membrane potential of Vero cells exposed to increasing concentrations of NaCl was determined by plate microfluorimetry recordings with the FlexStation III microplate reader and the FLIPR Membrane Potential Assay Kit (Molecular Devices Corp., Sunnyvale, CA) following the manufacturer's instructions, as previously described.[68] The kit provides results in good correlation with those obtained in patch-clamping assays. Recordings of the fluorescence intensity of 5×10^4 cells in black, clear-bottom, 96-well plates were acquired at rest (point 0 h), 1 h, 24 h, or 72 h after NaCl challenge (depolarizing agent). Cells, exposed to NaCl in parallel assays for 0−72 h, were then incubated with the Membrane Potential Kit for 1 h at 37 °C before measurements. Each preparation was only used for one time point measurement. In the case of real time kinetics assays, the cells were previously incubated with the Membrane Potential Kit for 1 h at 37 °C, and then the cells were treated with different concentrations of NaCl and the fluorescence measurements performed for 120 s at 1.52 s intervals. Basal fluorescence intensity was measured for 30 s. Responses were calculated as the peak fluorescence minus the basal fluorescence. Fluorescence intensity was determined using the SoftMax2Pro software (Molecular Devices).

Analysis of Changes of $[Ca^{2+}]_i$ by Microfluorimetry. Variation of intracellular free calcium concentrations ($[Ca^{2+}]_i$) of Vero cells exposed to increasing concentrations of NaCl was determined by plate microfluorimetry recordings with the FlexStation III microplate reader and the FLIPR Calcium 4l Assay Kit (Molecular Devices Corp., Sunnyvale, CA) following the manufacturer's instructions, as previously described.[68] Recordings of the fluorescence intensity of 5×10^4 cells in black clear-bottom 96-well plates were acquired by measuring at 1.52 s intervals for 120 s after 15 s of monitoring basal fluorescence intensity. Responses were calculated as the peak fluorescence minus the basal fluorescence. Fluorescence intensity was determined using the SoftMax2Pro software (Molecular Devices).

Analysis of Mitochondrial Function through Oxygen Consumption Rate and Extracellular Acidification Rate. The oxygen consumption rate (OCR) and extracellular acidification rate (ECAR) were measured using the Seahorse XFe24 Analyzer (Agilent Technologies). XFe24 plates were seeded with 40 000 Vero cells per well. After 24 h, the culture medium was replaced with a medium containing the NaCl treatment (110, 135, 160, 185, 210, 235, 260, 280 mM final concentration) and incubated for 72 h. The medium utilized for OCR and ECAR experiments was DMEM high glucose (Gibco, Thermo Fisher) without sodium bicarbonate and FBS. Cells were then incubated for 1 h at 37 °C. Four compounds were used for the Seahorse XF Cell Mito Stress Test and injected during the assay at the following final concentrations: oligomycin (1 μg/mL), CCCP (2 μM), and rotenone (1 μM) plus antimycin A (1 μg/mL). Mitochondrial respiration was evaluated under four different conditions: *basal respiration*, corresponding to the cell basal oxygen consumption, without the addition of substrates or inhibitors; *proton leak*, after oligomycin (ATP-synthase blocker) addition, where oxygen consumption occurs due mitochondrial inner membrane proton leak; *uncoupled*, after the addition of respiratory chain uncoupler CCCP, where the oxygen consumed reflects the maximal respiration rate (irreversibly uncoupling from ATP synthesis); and *inhibited*, with the addition of rotenone (complex I blocker) and antimycin (complex III blocker), where the oxygen consumption reflects nonmitochondrial activity. The ECAR rate was verified through application of the glycolysis stress test kit (Agilent Technologies). Agilent Seahorse Wave 2.6.1 software was used for data analysis.

ATP Detection Luciferase Assay. Changes of the total concentration of ATP in Vero cells exposed to increasing concentrations of NaCl for 1 or 72 h was determined by plate microfluorimetry recordings with the FlexStation III microplate reader and the ATP Assay Kit (SIGMA-Aldrich) following the manufacturer's instructions, as previously described.[68] The kit provides sensitive results, detecting ATP release of 10−100 mammalian cells/well, based on the firefly luciferase-catalyzed oxidation of D-luciferin in the presence of ATP, in which the amount of ATP is quantified by the amount of light ($h\nu$) produced. Recordings of the luminescence intensity of 5×10^4 cells in black clear-bottom 96-well plates were acquired at rest (point 0 h) and 1 and 72 h after NaCl challenge (depolarizing agent). Time kinetics were obtained by measuring at 1.52 s intervals for 120 s after 10 s of monitoring basal fluorescence intensity, which is the luminescence emission rate prior to addition of the ATP-releasing agent. Responses were calculated as the peak luminescence minus the

https://doi.org/10.1021/acsptsci.1c00080
ACS Pharmacol. Transl. Sci. XXXX, XXX, XXX−XXX

basal luminescence, using the SoftMax2Pro software (Molecular Devices).

Statistical Analysis. Data were expressed as mean values ± SEM (standard error of the mean) of three independent experiments, with each measure performed in triplicate. Percentages of inhibition and cytotoxicity were calculated and normalized to untreated (110 mM NaCl) cells. p values were calculated using an unpaired two-tailed t test or one-way ANOVA, when appropriate. $p \leq 0.05$ was considered significant. The data were analyzed, and the graphics were designed using GraphPad Prism 8.4.1 software.

AUTHOR INFORMATION

Corresponding Authors

Cristiane Rodrigues Guzzo − *Department of Microbiology, Institute of Biomedical Sciences, University of São Paulo, São Paulo 05508, Brazil;* orcid.org/0000-0002-5664-8055; Email: crisguzzo@usp.br

Edison L. Durigon − *Department of Microbiology, Institute of Biomedical Sciences, University of São Paulo, São Paulo 05508, Brazil; Scientific Platform Pasteur USP, São Paulo 05508, Brazil*; Email: eldurigo@usp.br

Henning Ulrich − *Department of Biochemistry, Institute of Chemistry, University of São Paulo, São Paulo 05508, Brazil;* orcid.org/0000-0002-2114-3815; Email: henning@iq.usp.br

Authors

Rafael R. G. Machado − *Department of Microbiology, Institute of Biomedical Sciences, University of São Paulo, São Paulo 05508, Brazil*

Talita Glaser − *Department of Biochemistry, Institute of Chemistry, University of São Paulo, São Paulo 05508, Brazil*

Danielle B. Araujo − *Department of Microbiology, Institute of Biomedical Sciences, University of São Paulo, São Paulo 05508, Brazil; Hospital Israelita Albert Einstein, São Paulo 05652, Brazil*

Lyvia Lintzmaier Petiz − *Department of Biochemistry, Institute of Chemistry, University of São Paulo, São Paulo 05508, Brazil*

Danielle B. L. Oliveira − *Department of Microbiology, Institute of Biomedical Sciences, University of São Paulo, São Paulo 05508, Brazil; Hospital Israelita Albert Einstein, São Paulo 05652, Brazil; Development and Innovation Center, Laboratory of Virology, Butantan Institute, São Paulo 05503, Brazil*

Giuliana S. Durigon − *Medical School Clinical Hospital, University of São Paulo, São Paulo 05508, Brazil*

Alessandra L. Leal − *Gaspar Vianna Clinic Hospital Foundation, Belém 66083, Brazil*

João Renato R. Pinho − *Hospital Israelita Albert Einstein, São Paulo 05652, Brazil; LIM-03, Central Laboratories Division, Clinics Hospital, São Paulo School of Medicine, University of São Paulo, São Paulo 05508, Brazil; LIM-07, Institute of Tropical Medicine, Department of Gastroenterology, University of São Paulo School of Medicine, São Paulo 05508, Brazil*

Luis C. S. Ferreira − *Department of Microbiology, Institute of Biomedical Sciences, University of São Paulo, São Paulo 05508, Brazil; Scientific Platform Pasteur USP, São Paulo 05508, Brazil*

Complete contact information is available at: https://pubs.acs.org/10.1021/acsptsci.1c00080

Author Contributions

¶Both authors contributed equally

Notes

The authors declare no competing financial interest.

ACKNOWLEDGMENTS

This work was supported by grants of the São Paulo Research Foundation (FAPESP Projects No. 2018/07366-4, 2019/00195-2, 2020/04680-0, 2017/24769-2, 2020/06409-1, 2016/20045-7, and 2020/06409-1), Coordenação de Aperfeiçoamento de Pessoal de Nível Superior (CAPES number 88887.131387/2016-00), and Rede Virus MCTI (grant FINEP 0459/20).

REFERENCES

(1) Zhu, N.; Zhang, D.; Wang, W.; Li, X.; Yang, B.; Song, J.; Zhao, X.; Huang, B.; Shi, W.; Lu, R.; Niu, P.; Zhan, F.; Ma, X.; Wang, D.; Xu, W.; Wu, G.; Gao, G. F.; Tan, W. China Novel Coronavirus Investigating and Research Team. A Novel Coronavirus from Patients with Pneumonia in China, 2019. *N. Engl. J. Med.* **2020**, *382* (8), 727−733.

(2) Karim, S. S. A. Vaccines and SARS-CoV-2 Variants: The Urgent Need for a Correlate of Protection. *Lancet* **2021**, *397* (10281), 1263−1264.

(3) Abdool Karim, S. S.; de Oliveira, T. New SARS-CoV-2 Variants — Clinical, Public Health, and Vaccine Implications. *N. Engl. J. Med.* **2021**, *384*, 1866−1868.

(4) Letko, M.; Marzi, A.; Munster, V. Functional Assessment of Cell Entry and Receptor Usage for SARS-CoV-2 and Other Lineage B Betacoronaviruses. *Nat. Microbiol* **2020**, *5* (4), 562−569.

(5) Wang, K.; Chen, W.; Zhang, Z.; Deng, Y.; Lian, J.-Q.; Du, P.; Wei, D.; Zhang, Y.; Sun, X.-X.; Gong, L.; Yang, X.; He, L.; Zhang, L.; Yang, Z.; Geng, J.-J.; Chen, R.; Zhang, H.; Wang, B.; Zhu, Y.-M.; Nan, G.; Jiang, J.-L.; Li, L.; Wu, J.; Lin, P.; Huang, W.; Xie, L.; Zheng, Z.-H.; Zhang, K.; Miao, J.-L.; Cui, H.-Y.; Huang, M.; Zhang, J.; Fu, L.; Yang, X.-M.; Zhao, Z.; Sun, S.; Gu, H.; Wang, Z.; Wang, C.-F.; Lu, Y.; Liu, Y.-Y.; Wang, Q.-Y.; Bian, H.; Zhu, P.; Chen, Z.-N. CD147-Spike Protein Is a Novel Route for SARS-CoV-2 Infection to Host Cells. *Signal Transduct Target Ther* **2020**, *5* (1), 283.

(6) Bò, L.; Miotto, M.; Di Rienzo, L.; Milanetti, E.; Ruocco, G. Exploring the Association Between Sialic Acid and SARS-CoV-2 Spike Protein Through a Molecular Dynamics-Based Approach. *Front. Med. Technol.* **2021**, *2*, 2.

(7) Baker, A. N.; Richards, S.-J.; Guy, C. S.; Congdon, T. R.; Hasan, M.; Zwetsloot, A. J.; Gallo, A.; Lewandowski, J. R.; Stansfeld, P. J.; Straube, A.; Walker, M.; Chessa, S.; Pergolizzi, G.; Dedola, S.; Field, R. A.; Gibson, M. I. The SARS-COV-2 Spike Protein Binds Sialic Acids, and Enables Rapid Detection in a Lateral Flow Point of Care Diagnostic Device. *ACS Cent. Sci.* **2020**, *6*, 2046.

(8) Jeffers, S. A.; Tusell, S. M.; Gillim-Ross, L.; Hemmila, E. M.; Achenbach, J. E.; Babcock, G. J.; Thomas, W. D.; Thackray, L. B.; Young, M. D.; Mason, R. J.; Ambrosino, D. M.; Wentworth, D. E.; DeMartini, J. C.; Holmes, K. V. CD209L (L-SIGN) Is a Receptor for Severe Acute Respiratory Syndrome Coronavirus. *Proc. Natl. Acad. Sci. U. S. A.* **2004**, *101* (44), 15748−15753.

(9) Yang, Z.-Y.; Huang, Y.; Ganesh, L.; Leung, K.; Kong, W.-P.; Schwartz, O.; Subbarao, K.; Nabel, G. J. pH-Dependent Entry of Severe Acute Respiratory Syndrome Coronavirus Is Mediated by the Spike Glycoprotein and Enhanced by Dendritic Cell Transfer through DC-SIGN. *J. Virol.* **2004**, *78* (11), 5642−5650.

(10) Hoffmann, M.; Kleine-Weber, H.; Schroeder, S.; Krüger, N.; Herrler, T.; Erichsen, S.; Schiergens, T. S.; Herrler, G.; Wu, N.-H.; Nitsche, A.; Müller, M. A.; Drosten, C.; Pöhlmann, S. SARS-CoV-2 Cell Entry Depends on ACE2 and TMPRSS2 and Is Blocked by a Clinically Proven Protease Inhibitor. *Cell* **2020**, *181* (2), 271−280.

(11) Li, F. Structure, Function, and Evolution of Coronavirus Spike Proteins. *Annu. Rev. Virol.* **2016**, *3* (1), 237−261.

(12) Bosch, B. J.; van der Zee, R.; de Haan, C. A. M.; Rottier, P. J. M. The Coronavirus Spike Protein Is a Class I Virus Fusion Protein: Structural and Functional Characterization of the Fusion Core Complex. *J. Virol.* **2003**, *77* (16), 8801−8811.
(13) Wrapp, D.; Wang, N.; Corbett, K. S.; Goldsmith, J. A.; Hsieh, C.-L.; Abiona, O.; Graham, B. S.; McLellan, J. S. Cryo-EM Structure of the 2019-nCoV Spike in the Prefusion Conformation. *Science* **2020**, *367* (6483), 1260−1263.
(14) Lan, J.; Ge, J.; Yu, J.; Shan, S.; Zhou, H.; Fan, S.; Zhang, Q.; Shi, X.; Wang, Q.; Zhang, L.; Wang, X. Structure of the SARS-CoV-2 Spike Receptor-Binding Domain Bound to the ACE2 Receptor. *Nature* **2020**, *581* (7807), 215−220.
(15) Silva de Souza, A.; Rivera, J. D.; Almeida, V. M.; Ge, P.; de Souza, R. F.; Farah, C. S.; Ulrich, H.; Marana, S. R.; Salinas, R. K.; Guzzo, C. R. Molecular Dynamics Reveals Complex Compensatory Effects of Ionic Strength on the Severe Acute Respiratory Syndrome Coronavirus 2 Spike/Human Angiotensin-Converting Enzyme 2 Interaction. *J. Phys. Chem. Lett.* **2020**, *11* (24), 10446−10453.
(16) Speir, R. W. Effect of Several Inorganic Salts on Infectivity of Mengo Virus. *Exp. Biol. Med.* **1961**, *106* (2), 402−404.
(17) Ramalingam, S.; Cai, B.; Wong, J.; Twomey, M.; Chen, R.; Fu, R. M.; Boote, T.; McCaughan, H.; Griffiths, S. J.; Haas, J. G. Antiviral Innate Immune Response in Non-Myeloid Cells Is Augmented by Chloride Ions via an Increase in Intracellular Hypochlorous Acid Levels. *Sci. Rep.* **2018**, *8* (1), 13630.
(18) Ramalingam, S.; Graham, C.; Dove, J.; Morrice, L.; Sheikh, A. A Pilot, Open Labelled, Randomised Controlled Trial of Hypertonic Saline Nasal Irrigation and Gargling for the Common Cold. *Sci. Rep.* **2019**, *9* (1), 1015.
(19) Chu, H.; Chan, J. F.-W.; Yuen, T. T.-T.; Shuai, H.; Yuan, S.; Wang, Y.; Hu, B.; Yip, C. C.-Y.; Tsang, J. O.-L.; Huang, X.; Chai, Y.; Yang, D.; Hou, Y.; Chik, K. K.-H.; Zhang, X.; Fung, A. Y.-F.; Tsoi, H.-W.; Cai, J.-P.; Chan, W.-M.; Ip, J. D.; Chu, A. W.-H.; Zhou, J.; Lung, D. C.; Kok, K.-H.; To, K. K.-W.; Tsang, O. T.-Y.; Chan, K.-H.; Yuen, K.-Y. Comparative Tropism, Replication Kinetics, and Cell Damage Profiling of SARS-CoV-2 and SARS-CoV with Implications for Clinical Manifestations, Transmissibility, and Laboratory Studies of COVID-19: An Observational Study. *Lancet Microbe* **2020**, *1* (1), e14−e23.
(20) Hoffmann, M.; Mösbauer, K.; Hofmann-Winkler, H.; Kaul, A.; Kleine-Weber, H.; Krüger, N.; Gassen, N. C.; Müller, M. A.; Drosten, C.; Pöhlmann, S. Chloroquine Does Not Inhibit Infection of Human Lung Cells with SARS-CoV-2. *Nature* **2020**, *585* (7826), 588−590.
(21) Xia, S.; Wu, M.; Chen, S.; Zhang, T.; Ye, L.; Liu, J.; Li, H. Long Term Culture of Human Kidney Proximal Tubule Epithelial Cells Maintains Lineage Functions and Serves as an Ex Vivo Model for Coronavirus Associated Kidney Injury. *Virol. Sin.* **2020**, *35* (3), 311−320.
(22) Ji, H.-L.; Song, W.; Gao, Z.; Su, X.-F.; Nie, H.-G.; Jiang, Y.; Peng, J.-B.; He, Y.-X.; Liao, Y.; Zhou, Y.-J.; Tousson, A.; Matalon, S. SARS-CoV Proteins Decrease Levels and Activity of Human ENaC via Activation of Distinct PKC Isoforms. *Am. J. Physiol. Lung Cell. Mol. Physiol.* **2009**, *296* (3), L372−L383.
(23) Xu, W.; Hong, S. J.; Zhong, A.; Xie, P.; Jia, S.; Xie, Z.; Zeitchek, M.; Niknam-Bienia, S.; Zhao, J.; Porterfield, D. M.; Surmeier, D. J.; Leung, K. P.; Galiano, R. D.; Mustoe, T. A. Sodium Channel Nax Is a Regulator in Epithelial Sodium Homeostasis. *Sci. Transl. Med.* **2015**, *7* (312), 312ra177.
(24) Ding, L.; Jiang, P.; Xu, X.; Lu, W.; Yang, C.; Li, L.; Zhou, P.; Liu, S. T-Type Calcium Channels Blockers Inhibit HSV-2 Infection at the Late Stage of Genome Replication. *Eur. J. Pharmacol.* **2021**, *892*, 173782.
(25) Son, Y. K.; Hong, D. H.; Li, H.; Kim, D.-J.; Na, S. H.; Park, H.; Jung, W.-K.; Choi, I.-W.; Park, W. S. Ca2+ Channel Inhibitor NNC 55−0396 Inhibits Voltage-Dependent K+ Channels in Rabbit Coronary Arterial Smooth Muscle Cells. *J. Pharmacol. Sci.* **2014**, *125* (3), 312−319.
(26) Hafting, T.; Sand, O. Purinergic Activation of BK Channels in Clonal Kidney Cells (Vero Cells). *Acta Physiol. Scand.* **2000**, *170* (2), 99−109.
(27) Nagy, P. D.; Lin, W. Taking over Cellular Energy-Metabolism for TBSV Replication: The High ATP Requirement of an RNA Virus within the Viral Replication Organelle. *Viruses* **2020**, *12* (1), 56.
(28) Copp, J.; Wiley, S.; Ward, M. W.; van der Geer, P. Hypertonic Shock Inhibits Growth Factor Receptor Signaling, Induces Caspase-3 Activation, and Causes Reversible Fragmentation of the Mitochondrial Network. *Am. J. Physiol. Cell Physiol.* **2005**, *288* (2), C403−C415.
(29) Mookerjee, S. A.; Goncalves, R. L. S.; Gerencser, A. A.; Nicholls, D. G.; Brand, M. D. The Contributions of Respiration and Glycolysis to Extracellular Acid Production. *Biochim. Biophys. Acta, Bioenerg.* **2015**, *1847* (2), 171−181.
(30) Dykens, J. A.; Will, Y. The Significance of Mitochondrial Toxicity Testing in Drug Development. *Drug Discovery Today* **2007**, *12* (17−18), 777−785.
(31) Cheung, P. W.; Bouley, R.; Brown, D. Targeting the Trafficking of Kidney Water Channels for Therapeutic Benefit. *Annu. Rev. Pharmacol. Toxicol.* **2020**, *60*, 175−194.
(32) Mohan, A.; Agarwal, S.; Clauss, M.; Britt, N. S.; Dhillon, N. K. Extracellular Vesicles: Novel Communicators in Lung Diseases. *Respir. Res.* **2020**, *21* (1), 175.
(33) Wang, H.; Yang, P.; Liu, K.; Guo, F.; Zhang, Y.; Zhang, G.; Jiang, C. SARS Coronavirus Entry into Host Cells through a Novel Clathrin- and Caveolae-Independent Endocytic Pathway. *Cell Res.* **2008**, *18* (2), 290−301.
(34) Ye, Q.; Wang, B.; Mao, J. The Pathogenesis and Treatment of the`Cytokine Storm' in COVID-19. *J. Infect.* **2020**, *80* (6), 607−613.
(35) Hummler, E.; Barker, P.; Gatzy, J.; Beermann, F.; Verdumo, C.; Schmidt, A.; Boucher, R.; Rossier, B. C. Early Death due to Defective Neonatal Lung Liquid Clearance in Alpha-ENaC-Deficient Mice. *Nat. Genet.* **1996**, *12* (3), 325−328.
(36) Matalon, S.; Lazrak, A.; Jain, L.; Eaton, D. C. Invited Review: Biophysical Properties of Sodium Channels in Lung Alveolar Epithelial Cells. *J. Appl. Physiol.* **2002**, *93* (5), 1852−1859.
(37) Matalon, S.; O'Brodovich, H. Sodium Channels in Alveolar Epithelial Cells: Molecular Characterization, Biophysical Properties, and Physiological Significance. *Annu. Rev. Physiol.* **1999**, *61*, 627−661.
(38) Kunzelmann, K.; Beesley, A. H.; King, N. J.; Karupiah, G.; Young, J. A.; Cook, D. I. Influenza Virus Inhibits Amiloride-Sensitive Na+ Channels in Respiratory Epithelia. *Proc. Natl. Acad. Sci. U. S. A.* **2000**, *97* (18), 10282−10287.
(39) Hoffmann, H.-H.; Palese, P.; Shaw, M. L. Modulation of Influenza Virus Replication by Alteration of Sodium Ion Transport and Protein Kinase C Activity. *Antiviral Res.* **2008**, *80* (2), 124−134.
(40) Lewis, S. A. Influenza Influences Ion Channels. *J. Physiol.* **2009**, *587* (13), 3055.
(41) Hover, S.; Foster, B.; Barr, J. N.; Mankouri, J. Viral Dependence on Cellular Ion Channels - an Emerging Anti-Viral Target? *J. Gen. Virol.* **2017**, *98* (3), 345−351.
(42) PLOS ONE Staff.. Correction: Channel Properties of Nax Expressed in Neurons. *PLoS One* **2015**, *10* (6), No. e0130107.
(43) Svenningsen, P.; Andersen, H.; Nielsen, L. H.; Jensen, B. L. Urinary Serine Proteases and Activation of ENaC in Kidney—implications for Physiological Renal Salt Handling and Hypertensive Disorders with Albuminuria. *Pfluegers Arch.* **2015**, *467*, 531−542.
(44) Bruns, J. B.; Carattino, M. D.; Sheng, S.; Maarouf, A. B.; Weisz, O. A.; Pilewski, J. M.; Hughey, R. P.; Kleyman, T. R. Epithelial Na+ Channels Are Fully Activated by Furin- and Prostasin-Dependent Release of an Inhibitory Peptide from the Gamma-Subunit. *J. Biol. Chem.* **2007**, *282* (9), 6153−6160.
(45) Marunaka, Y.; Marunaka, R.; Sun, H.; Yamamoto, T.; Kanamura, N.; Taruno, A. Na Homeostasis by Epithelial Na Channel (ENaC) and Nax Channel (Nax): Cooperation of ENaC and Nax. *Annals of Translational Medicine* **2016**, *4*, S11−S11.
(46) Berka, U.; Khan, A.; Blaas, D.; Fuchs, R. Human Rhinovirus Type 2 Uncoating at the Plasma Membrane Is Not Affected by a pH

https://doi.org/10.1021/acsptsci.1c00080
ACS Pharmacol. Transl. Sci. XXXX, XXX, XXX−XXX

Gradient but Is Affected by the Membrane Potential. *J. Virol.* **2009**, *83*, 3778−3787.
(47) Song, W.; Liu, G.; Bosworth, C. A.; Walker, J. R.; Megaw, G. A.; Lazrak, A.; Abraham, E.; Sullender, W. M.; Matalon, S. Respiratory Syncytial Virus Inhibits Lung Epithelial Na+ Channels by up-Regulating Inducible Nitric-Oxide Synthase. *J. Biol. Chem.* **2009**, *284* (11), 7294−7306.
(48) Koshiba, T.; Yasukawa, K.; Yanagi, Y.; Kawabata, S.-I. Mitochondrial Membrane Potential Is Required for MAVS-Mediated Antiviral Signaling. *Sci. Signaling* **2011**, *4* (158), No. ra7.
(49) Gorman, G. S.; Chinnery, P. F.; DiMauro, S.; Hirano, M.; Koga, Y.; McFarland, R.; Suomalainen, A.; Thorburn, D. R.; Zeviani, M.; Turnbull, D. M. Mitochondrial Diseases. *Nat. Rev. Dis Primers* **2016**, *2*, 16080.
(50) Zou, L.; Ruan, F.; Huang, M.; Liang, L.; Huang, H.; Hong, Z.; Yu, J.; Kang, M.; Song, Y.; Xia, J.; Guo, Q.; Song, T.; He, J.; Yen, H.-L.; Peiris, M.; Wu, J. SARS-CoV-2 Viral Load in Upper Respiratory Specimens of Infected Patients. *N. Engl. J. Med.* **2020**, *382* (12), 1177−1179.
(51) Figueroa, J. M.; Primrose, D.; Vdugour, A.; Ochoa, V.; Bitler, J.; Erra Diaz, F. Effect of Hypertonic Saline Solution on Cultures of Human Respiratory Epithelium Infected by Respiratory Syncytial Virus. In *Airway Cell Biology and Immunopathology*; European Respiratory Society, 2018. DOI: 10.1183/13993003.congress-2018.pa4978.
(52) Zhang, W.-C.; Du, L.-J.; Zheng, X.-J.; Chen, X.-Q.; Shi, C.; Chen, B.-Y.; Sun, X.-N.; Li, C.; Zhang, Y.-Y.; Liu, Y.; Xiao, H.; Leng, Q.; Jiang, X.; Zhang, Z.; Sun, S.; Duan, S.-Z. Elevated Sodium Chloride Drives Type I Interferon Signaling in Macrophages and Increases Antiviral Resistance. *J. Biol. Chem.* **2018**, *293* (3), 1030−1039.
(53) Elkins, M. R.; Robinson, M.; Rose, B. R.; Harbour, C.; Moriarty, C. P.; Marks, G. B.; Belousova, E. G.; Xuan, W.; Bye, P. T. P. National Hypertonic Saline in Cystic Fibrosis (NHSCF) Study Group. A Controlled Trial of Long-Term Inhaled Hypertonic Saline in Patients with Cystic Fibrosis. *N. Engl. J. Med.* **2006**, *354* (3), 229−240.
(54) Zhang, L.; Mendoza-Sassi, R. A.; Wainwright, C.; Klassen, T. P. Nebulised Hypertonic Saline Solution for Acute Bronchiolitis in Infants. *Cochrane Database Syst. Rev.* **2017**, *12*, CD006458.
(55) Luo, Z.; Fu, Z.; Liu, E.; Xu, X.; Fu, X.; Peng, D.; Liu, Y.; Li, S.; Zeng, F.; Yang, X. Nebulized Hypertonic Saline Treatment in Hospitalized Children with Moderate to Severe Viral Bronchiolitis. *Clin. Microbiol. Infect.* **2011**, *17* (12), 1829−1833.
(56) Rabago, D.; Zgierska, A. Saline Nasal Irrigation for Upper Respiratory Conditions. *Am. Fam. Physician* **2009**, *80* (10), 1117−1119.
(57) Ramalingam, S.; Graham, C.; Dove, J.; Morrice, L.; Sheikh, A. Hypertonic Saline Nasal Irrigation and Gargling Should Be Considered as a Treatment Option for COVID-19. *J. Glob. Health* **2020**, *10* (1), 010332.
(58) Casale, M.; Rinaldi, V.; Sabatino, L.; Moffa, A.; Ciccozzi, M. Could Nasal Irrigation and Oral Rinse Reduce the Risk for COVID-19 Infection? *Int. J. Immunopathol. Pharmacol.* **2020**, *34*, 2058738420941757.
(59) Farrell, N. F.; Klatt-Cromwell, C.; Schneider, J. S. Benefits and Safety of Nasal Saline Irrigations in a Pandemic-Washing COVID-19 Away. *JAMA Otolaryngol. Head Neck Surg.* **2020**, *146* (9), 787−788.
(60) Araujo, D. B.; Machado, R. R. G.; Amgarten, D. E.; Malta, F. de M.; de Araujo, G. G.; Monteiro, C. O.; Candido, E. D.; Soares, C. P.; de Menezes, F. G.; Pires, A. C. C.; Santana, R. A. F.; Viana, A. de O.; Dorlass, E.; Thomazelli, L.; Ferreira, L. C. de S.; Botosso, V. F.; Carvalho, C. R. G.; Oliveira, D. B. L.; Pinho, J. R. R.; Durigon, E. L. SARS-CoV-2 Isolation from the First Reported Patients in Brazil and Establishment of a Coordinated Task Network. *Mem. Inst. Oswaldo Cruz* **2020**, *115*, No. e200342.
(61) Preparedness, E. Laboratory biosafety guidance related to coronavirus disease (COVID-19). https://www.who.int/publications/i/item/laboratory-biosafety-guidance-related-to-coronavirus-disease-(covid-19) (accessed May 18, 2021).
(62) Wang, M.; Cao, R.; Zhang, L.; Yang, X.; Liu, J.; Xu, M.; Shi, Z.; Hu, Z.; Zhong, W.; Xiao, G. Remdesivir and Chloroquine Effectively Inhibit the Recently Emerged Novel Coronavirus (2019-nCoV) in Vitro. *Cell Res.* **2020**, *30* (3), 269−271.
(63) Corman, V. M.; Landt, O.; Kaiser, M.; Molenkamp, R.; Meijer, A.; Chu, D. K.; Bleicker, T.; Brünink, S.; Schneider, J.; Schmidt, M. L.; Mulders, D. G.; Haagmans, B. L.; van der Veer, B.; van den Brink, S.; Wijsman, L.; Goderski, G.; Romette, J.-L.; Ellis, J.; Zambon, M.; Peiris, M.; Goossens, H.; Reusken, C.; Koopmans, M. P.; Drosten, C. Detection of 2019 Novel Coronavirus (2019-nCoV) by Real-Time RT-PCR. *Euro Surveill.* **2020**, *25* (3), DOI: 10.2807/1560-7917.ES.2020.25.3.2000045.
(64) Drosten, C.; Günther, S.; Preiser, W.; van der Werf, S.; Brodt, H.-R.; Becker, S.; Rabenau, H.; Panning, M.; Kolesnikova, L.; Fouchier, R. A. M.; Berger, A.; Burguière, A.-M.; Cinatl, J.; Eickmann, M.; Escriou, N.; Grywna, K.; Kramme, S.; Manuguerra, J.-C.; Müller, S.; Rickerts, V.; Stürmer, M.; Vieth, S.; Klenk, H.-D.; Osterhaus, A. D. M. E.; Schmitz, H.; Doerr, H. W. Identification of a Novel Coronavirus in Patients with Severe Acute Respiratory Syndrome. *N. Engl. J. Med.* **2003**, *348* (20), 1967−1976.
(65) Sales-Medina, D. F.; Ferreira, L. R. P.; Romera, L. M. D.; Gonçalves, K. R.; Guido, R. V. C.; Courtemanche, G.; Buckeridge, M. S.; Durigon, É. L.; Moraes, C. B.; Freitas-Junior, L. H. Discovery of Clinically Approved Drugs Capable of Inhibiting SARS-CoV-2 in Vitro Infection Using a Phenotypic Screening Strategy and Network-Analysis to Predict Their Potential to Treat Covid-19. *bioRxiv* **2020**, DOI: 10.1101/2020.07.09.196337.
(66) ISO 10993-5:2009 https://www.iso.org/cms/render/live/en/sites/isoorg/contents/data/standard/03/64/36406.html (accessed May 18, 2021).
(67) Belloc, F.; Dumain, P.; Boisseau, M. R.; Jalloustre, C.; Reiffers, J.; Bernard, P.; Lacombe, F. A Flow Cytometric Method Using Hoechst 33342 and Propidium Iodide for Simultaneous Cell Cycle Analysis and Apoptosis Determination in Unfixed Cells. *Cytometry* **1994**, *17* (1), 59−65.
(68) Glaser, T.; Shimojo, H.; Ribeiro, D. E.; Martins, P. P. L.; Beco, R. P.; Kosinski, M.; Sampaio, V. F. A.; Corrêa-Velloso, J.; Oliveira-Giacomelli, Á.; Lameu, C.; de Jesus Santos, A. P.; de Souza, H. D. N.; Teng, Y. D.; Kageyama, R.; Ulrich, H. ATP and Spontaneous Calcium Oscillations Control Neural Stem Cell Fate Determination in Huntington's Disease: A Novel Approach for Cell Clock Research. *Mol. Psychiatry* **2020**, DOI: 10.1038/s41380-020-0717-5.

https://doi.org/10.1021/acsptsci.1c00080
ACS Pharmacol. Transl. Sci. XXXX, XXX, XXX−XXX